Neptune's HCl upper limit from Herschel/HIFI[☆]

N. A. Teanby[a], B. Gould[a], P. G. J. Irwin[b]

[a]*School of Earth Sciences, University of Bristol, Wills Memorial Building, Queens Road, Bristol, BS8 1RJ, U.K.*
[b]*Atmospheric, Oceanic & Planetary Physics, Department of Physics, University of Oxford, Clarendon Laboratory, Parks Road, Oxford, OX1 3PU. UK.*

Abstract

Here we search for hydrogen chloride (HCl) in Neptune's stratosphere using observations of the 1876.22 GHz J=3–2 transition from the Heterodyne Instrument for the Far-Infrared (HIFI) on Herschel. Observations comprise a 7.2 hr disc-averaged integration, originally designed to investigate stratospheric methane. Significant HCl emission was not detected. Instead, we determine upper limits using step-type abundance profiles, defined by zero deep abundance and uniform volume mixing ratio for pressures less than a transition pressure (assumed to be 0.1 or 1 mbar). These profiles are a reasonable first-order approximation for an externally sourced species; at higher pressures HCl is expected to be removed by aerosol scavenging and reactions with ammonia. The 3σ upper limits are <0.70 parts per billion (ppb) for a 0.1 mbar transition pressure and <0.076 ppb for a 1 mbar transition pressure. These upper limits are the most stringent to date and are consistent with current estimates of interplanetary dust particle flux and the hypothesis that

[☆] *Herschel* is an ESA space observatory with science instruments provided by European-led Principal Investigator consortia and with important participation from NASA.

Email address: n.teanby@bristol.ac.uk (N. A. Teanby)

Neptune experienced a large comet impact in the past 1000 years.

Keywords: Neptune, Atmosphere, Composition, Herschel, sub-millimetre

1. Introduction

Hydrogen chloride (HCl) provides an important probe of external flux and in-situ chemistry in giant planet atmospheres, but has so far not been detected on any of the giant planets. Therefore, in the absence of any detections, we start by considering Neptune's bulk chlorine abundance for context. Measurements from chondritic meteorites and observations of the Sun's photosphere suggest the solar Cl/H ratio is 1.8×10^{-7} (Lodders, 2010). If HCl were Neptune's dominant chlorine compound and assuming a molar He/H_2 ratio of 0.15 (Conrath et al., 1993), the implied bulk HCl volume mixing ratio would be 0.3 ppm (parts per million). However, Neptune is significantly enriched in heavy elements compared to the Sun, due to a more significant mass component being contributed from icy planetesimals during formation, rather than direct nebular gas capture (Owen and Encrenaz, 2006; Irwin, 2009; Fortney and Nettelmann, 2010; Helled et al., 2011; Nettelmann et al., 2013; Cavalié et al., 2020; Mousis et al., 2020; Atreya et al., 2020). This enrichment would result in a larger bulk chlorine abundance.

The exact magnitude of elemental enrichment in Neptune is currently uncertain, but can be estimated using observations of trace species in Neptune's observable atmosphere. This is challenging because the observable atmospheric composition may not be directly related to the interior composition due to many atmospheric and interior processes (Atreya et al., 2020; Cavalié et al., 2020; Teanby et al., 2020). These processes include: exter-

nal flux from micrometeorites and interplanetary dust particles (Moses and Poppe, 2017); comet impacts (Moreno et al., 2017; Lellouch et al., 2005); photochemical processing (Moses, 1992; Moses et al., 2018; Dobrijevic et al., 2020); internal thermochemical reactions (Lodders and Fegley, 1994; Cavalié et al., 2020; Venot et al., 2020); and uncertainty in mixing and equilibration processes in the deep interior (Helled and Stevenson, 2017; Helled et al., 2020).

Nevertheless, with caution some inferences from atmospheric observations can be made, assuming that the interior is well mixed. These are reviewed in detail by Teanby et al. (2020), with the key observations summarised briefly here. Observations of CH_4 abundances of 2–4% by volume, at pressures higher than the 1–2 bar condensation level, provide the most reliable indicator of internal enrichment currently available (Atreya et al., 2020; Cavalié et al., 2020; Mousis et al., 2020), and suggest a C/H enrichment of ∼50–100 (Baines et al., 1995; Karkoschka and Tomasko, 2011; Tollefson et al., 2019; Irwin et al., 2019a). Inferred interior water content derived from observations of D/H suggest an O/H enrichment of ∼50–150 (Feuchtgruber et al., 2013), but rely on assumptions about the D/H ratio in the source ices. CO observations imply even more extreme enrichments might be possible for O/H, with enrichments as high as 250–650 being suggested to explain to explain the presence of possibly internally-sourced CO in Neptune's troposphere (Lellouch et al., 2005; Luszcz-Cook and de Pater, 2013; Cavalié et al., 2017; Venot et al., 2020). Alternatively, if CO is externally sourced and only present in Neptune's stratosphere and upper troposphere because of downward mixing, O/H enrichments of ∼30–130 may be more reasonable (Teanby et al., 2019;

Teanby et al., 2020).

Given the variability and inconsistency of interior enrichment estimates, a conservative estimate of Neptune's bulk Cl/H enrichment is ∼50. This would imply a bulk HCl volume mixing ratio of ∼50×0.3 ppm = 15 ppm if all chlorine is in the form of HCl. Thermochemical models developed for Jupiter and Saturn's interiors show that HCl is only dominant at temperatures from ∼450–1500 K, corresponding to pressures of ∼200–10^5 bar (Fegley and Lodders, 1994). At higher pressures and temperatures, in the very deep interior, alkali chlorides such as NaCl are the dominant form of chlorine. At lower pressures and temperatures HCl reacts rapidly with NH_3 to form ammonium chloride salts (NH_4Cl), so is removed from the atmosphere (Fegley and Lodders, 1994; Showman, 2001). Showman (2001) estimates this loss process is extremely rapid, with a timescale of a few seconds or less, so an internal source for HCl is extremely unlikely.

Therefore, any HCl observed in Neptune's stratosphere must be external in origin and so provides constraints on stratospheric chemistry and external fluxes. Possible external sources include micrometeorites, interplanetary dust particles, and comet impacts (Moses and Poppe, 2017; Moreno et al., 2017). Stratospheric HCl should be stable to loss via ammonia salt creation as any residual NH_3 advected from the deep troposphere will be effectively removed by condensation, reactions with excess H_2S to form NH_4SH (Irwin et al., 2019b), and photolysis (Kaye and Strobel, 1983; Moses, 2000). However, other HCl loss processes such as aerosol scavenging provide alternative potentially efficient removal processes, but are not well constrained (Showman, 2001; Teanby et al., 2014). Therefore, observations of HCl provide important

constraints on external sources, loss processes, and photochemical pathways in Neptune's stratosphere.

Previous studies have searched for HCl on Jupiter (Fouchet et al., 2004; Teanby et al., 2014) and Saturn (Teanby et al., 2006; Fletcher et al., 2012), but have been unsuccessful. The current best 3σ upper limit for Jupiter is 0.061 ppb (parts per billion) (Teanby et al., 2014) and for Saturn is 130 ppb (Fletcher et al., 2012), assuming for both planets that HCl is confined to pressures less than 1 mbar. Neptune provides a promising target for HCl detection as it has the second highest interplanetary dust particle (IDP) flux after Jupiter (Moses and Poppe, 2017), a colder tropopause resulting in less stratospheric residual ammonia, and is thought to have recently experienced a large comet impact (Moreno et al., 2017).

Evidence for a recent comet impact is provided by observations of Neptune's stratospheric CO, where many studies have observed ∼1 ppm (parts per million) abundances (Lellouch et al., 2005; Marten et al., 2005; Hesman et al., 2007; Lellouch et al., 2010; Fletcher et al., 2010; Luszcz-Cook and de Pater, 2013; Teanby et al., 2019). This CO abundance is not compatible with the external steady IDP flux derived from modelling (Moses and Poppe, 2017) or inferred from the observed stratospheric H_2O abundance (Feuchtgruber et al., 1997), which also has an external origin. A possible explanation for abundant stratospheric CO is that Neptune has suffered a giant kilometre-scale comet impact in the last ∼1000 years, supplying significant external material directly into the stratosphere and producing CO from cometary H_2O via shock chemistry (Lellouch et al., 2005; Moreno et al., 2017). This would also explain recent observations of CS in Neptune's strato-

sphere (Moreno et al., 2017), another shock chemistry product, which was also observed on Jupiter in the wake of the SL9 impact (Lellouch, 1996). The disparate CO and H_2O observations suggest Neptune's stratospheric composition may not be in a steady-state and observing HCl could provide additional constraints on Neptune's external flux and chemistry.

The Herschel Space Telescope (Pilbratt et al., 2010) provides an excellent opportunity to search for strong sub-mm HCl lines due to its sensitive instrumentation and high spectral resolution. The Heterodyne Instrument for the Far-Infrared (HIFI) instrument (de Graauw et al., 2010) is particularly suitable for observing narrow emission lines from upper stratospheric gases. In this study we use HIFI observations to place new constraints on Neptune's stratospheric HCl abundance.

2. Observations

Observations were taken with Herschel's HIFI instrument. The Herschel Space Telescope is summarised in Pilbratt et al. (2010) and HIFI is explained in detail by de Graauw et al. (2010). Herschel's instruments rely on cryogenic cooling and were operational between 2009 and 2013. Over 44000 data products from the mission have been reduced and are now publicly available from the Herschel Science Archive (HSA[1]), although a small number ($\sim$1000) of calibration and engineering products remain restricted. We searched the HSA for any HIFI observations of Neptune that had a spectral range overlapping with any of HCl's sub-millimetre rotational lines. This revealed only one

[1] `http://archives.esac.esa.int/hsa/whsa/`

suitable observation: open time program (OT1) `OT1_rmoreno_2` (observation ID 1342233296) in band 7 covering a 2 GHz region around the 1882 GHz methane line (Moreno, 2010). This observation has been previously analysed to determine Neptune's CH_4 profile (Lellouch et al., 2015).

HIFI is a double side band (DSB) instrument, where two spectral ranges are covered simultaneously either side of a central local oscillator frequency, and combine into a single spectrum (de Graauw et al., 2010). Observations are designed to target specific species in either the upper side band (USB) or lower side band (LSB), with the other sideband ideally having no strong lines to simplify data analysis. However, sometimes unexpected detections may be possible using the other sideband. For example, HNC on Titan was first discovered this way using the LSB of an observation designed to study H_2O emission in the USB (Moreno et al., 2011).

The selected HIFI observation spans the spectral range 1881.3–1883.9 GHz in the upper side band (USB) covering the CH_4 emission features, but fortuitously also 1874.1–1876.7 GHz in the lower side band (LSB), including the HCl J=3–2 transition line at 1876.22GHz. The combined double side band (DSB) spectrum had a central local oscillator frequency of 1878.7950 GHz. The single side band efficiencies for the LSB and USB can be assumed to be 0.5 in band 7, so that LSB and USB spectral regions have equal weighting in the combined spectrum (Roelfsema et al., 2012). Total integration time was 25817 sec (7.2 hrs) starting at 06:21:22 on 29^{th} November 2011 (operational day 929) at a spectral resolution of 1.1 MHz with HIFI's wide-band spectrometer (WBS). HIFI's dual beam switch single point observation mode was used (HIFI Observers' Manual, 2011; Roelfsema et al., 2012) and data

were reduced using pipeline version SPG v14.1.0 to give separate horizontally and vertically polarised DSB spectra (Shipman et al., 2017). We use the Level 2.5 pipeline data products, which have been converted into physical units of antenna temperature (T_A), have individual sub-bands stitched together to give continuous spectra, and are Doppler corrected for relative motion between Neptune and Herschel.

HIFI band 7 observations are effected by electrical standing waves, which have a typical wavelength of 100 MHz. These standing waves are effectively removed using task `doHebCorrection` during pipeline processing (Shipman et al., 2017; Kester et al., 2014) and are not apparent in the Level 2.5 data. This processing is not expected to affect any real spectral features or the baseline level (Kester et al., 2014). The standing waves are also much longer wavelength than the expected narrow HCl emission features. At the time of the observation, Neptune had a relative velocity of 29.62 $\mathrm{km\,s^{-1}}$ away from Herschel, which meant the local oscillator had an effective frequency of 1878.9806 GHz in the Doppler corrected spectrum. Herschel's 3.28 m effective diameter primary mirror has an Airy disc diameter of 12.3 arcsec at 1875GHz - much larger than Neptune's apparent diameter of 2.27 arcsec - resulting in a disc-average spectrum. The Doppler corrected level 2.5 data are shown in Figure 1a.

The original 1.1 MHz resolution spectrum was re-binned to a 6 MHz resolution prior to analysis. This new resolution is still higher than the intrinsic line widths of spectral features in Neptune's spectrum (see section 3), so does not degrade the spectrum, but has advantages of: (1) providing an independent estimate of the uncertainty of each spectral point from the stan-

dard error of the points in each bin; and (2) reducing the number of spectral points, so making the spectral modelling more efficient. The re-binning also improve the signal-to-noise by a factor of $\sqrt{6/1.1} \sim 2.3$. However, the accuracy of any subsequent analysis is unchanged due to the reduced number of points in the re-binned spectrum. Antenna temperature was then converted to a line-to-continuum ratio by rescaling with the mean antenna temperature of the continuum after masking out the CH_4 emission lines and HCl line position. The advantage of rescaling the spectrum to a line-to-continuum ratio is that the data then becomes independent of beam efficiency and beam dilution due to the disc averaged nature of spectrum. Vertical and horizontal polarisations were averaged together to provide an overall spectrum for analysis mapped onto the LSB frequency axis. The final DSB binned line-to-continuum spectrum is shown in Figure 1b.

3. Spectral modelling

HIFI spectra were analysed using the NEMESIS radiative transfer code (Irwin et al., 2008). Our nominal Neptune atmospheric model is the same as that used by Teanby et al. (2019) and has a temperature profile based on Voyager radio occultations (Lindal, 1992) and AKIRI observations (Fletcher et al., 2010) (Figure 2a). Atmospheric gases that contribute to the 1875 GHz spectral region are H_2, He, N_2 and CH_4. We used a He/H_2 ratio of 0.15 by volume and an N_2 volume mixing ratio of 0.003 derived by Conrath et al. (1993) from Voyager infrared and radio observations. The CH_4 profile (Figure 2b) is from analysis by Lellouch et al. (2015) who use the same HIFI observations as those used here.

The overall effective instrument function of the HIFI DSB spectra is defined by a convolution of the original 1.1 MHz instrument function, the square 6 MHz width noise reducing bin, and Doppler rotation broadening caused by Neptune's rapid rotation and the disc-averaged nature of the spectrum. Following the method in Teanby et al. (2014), the Doppler rotation broadening has a full-width half-maximum (FWHM) of 25.6MHz. This Doppler broadening dominates the overall combined FWHM of 24.6MHz and the effect of the noise-reducing binning is negligible. For computational efficiency, pre-tabulated absorption parameters were calculated using the correlated-k approximation (Goody and Yung, 1989; Lacis and Oinas, 1991) and the instrument function was incorporated directly into the k-tables. Spectroscopic line parameters for the gases were the same at those used by Teanby et al. (2019).

To create a representative disc-average Neptune spectrum, an area-weighted average spectrum was generated from 33 annuli centred on Neptune with mean emission angles spanning Neptune's disc and limb; 20 on disc and 13 covering the limb (Teanby et al., 2019). This methodology is outlined in detail in Teanby et al. (2013). To allow a direct comparison with the measured HIFI data, the resulting synthetic spectrum is folded about the Doppler corrected local oscillator frequency and averaged with single side band weights of 0.5 (Roelfsema et al., 2012) to create a synthetic DSB spectrum. The same methane and HCl line masking was applied to the DSB synthetic as to the observations to convert the synthetic into a line-to-continuum ratio by rescaling with the mean continuum level.

To include HCl emission in the synthetic spectrum requires some knowl-

edge of its likely atmospheric profile. A uniform volume mixing ratio throughout the troposphere and stratosphere is not realistic as HCl will have been removed from the observable troposphere by reactions with ammonia in the deep atmosphere. A uniform abundance throughout the stratosphere is also not likely. Externally sourced HCl is likely to be most abundant in the upper stratosphere and mesosphere as maximum ablation of IDPs occurs at pressures less than ∼1–0.1 mbar (Moses and Poppe, 2017). In the middle and lower stratosphere of giant planets, scavenging of HCl by aerosols is expected to be an important removal process (Showman, 2001; Teanby et al., 2014). On Neptune, hazes are known to exist at pressures higher than ∼1 mbar (Irwin et al., 2011; Luszcz-Cook et al., 2016; Irwin et al., 2016; Moses et al., 1995), which suggests HCl is unlikely to be present in significant quantities in the lower stratosphere. Therefore, we consider the simplest appropriate profile of HCl to be a step function, with a uniform volume mixing ratio at pressures below 0.1 or 1 mbar and zero abundance at higher pressures (Figure 2c). These are similar to the profiles used by Teanby et al. (2014) for HCl on Jupiter and Moreno et al. (2017) for CS on Neptune. Nominal abundances of 1 ppb for the 0.1 mbar step and 0.1 ppb for the 1 mbar step were used to define the mask for the HCl emission line and as a starting point for the subsequent analysis.

4. Results

To determine if significant HCl was present in Neptune's stratosphere we created a suite of synthetic spectra with HCl abundances on a finely spaced grid from 0–1 ppb using both 1 and 0.1 mbar step function profiles. For each

synthetic spectrum with HCl abundance x the χ^2 misfit between observation $I_{\rm obs}(\nu_i)$ and synthetic $I_{\rm fit}(\nu_i, x)$ was calculated following the method outlined in Teanby et al. (2019):

$$\chi^2(x) \;=\; \frac{\Delta\nu_{\rm obs}}{\Delta\nu_{\rm res}} \sum_{i=1}^{N} \left[\frac{I_{\rm obs}(\nu_i) - I_{\rm fit}(\nu_i, x)}{\sigma(\nu_i)} \right]^2 \qquad (1)$$

where $\Delta\nu_{\rm obs}$ is the spacing of the binned data (6MHz), $\Delta\nu_{\rm res}$ is the observation spectral resolution (24.6MHz), and the observed spectrum has errors $\sigma(\nu_i)$ and is measured at N frequencies ν_i $(i = 1 \ldots N)$. The factor $\Delta\nu_{\rm obs}/\Delta\nu_{\rm res}$ is a modification to the usual χ^2 definition and accounts for the fact that the channel spacing is smaller than the effective spectral resolution, which means the effective number of independent spectral points is less than the number of channels by this factor. The significance of any detection is given by the change in χ^2 from the zero abundance case $\Delta\chi^2(x) = \chi^2(x) - \chi^2(0)$. From Press et al. (1992) a 1σ detection has $\Delta\chi^2(x) = -1$, a 2σ detection has $\Delta\chi^2(x) = -4$, a 3σ detection has $\Delta\chi^2(x) = -9$, and in the case of no detection a 3σ upper limit is given by $\Delta\chi^2(x) = +9$. We consider 3σ the threshold for a reliable detection.

Figure 3 shows the variation of $\Delta\chi^2$ with HCl volume mixing ratio for 1 and 0.1 mbar step profiles along with fits to the observed spectrum. The Lellouch et al. (2015) CH_4 profile fits the methane emission lines very well and to within errors, independently confirming the spectral fitting procedure. A small feature in the observed spectrum around the position of the HCl line results in a modest $\Delta\chi^2$ minima of -2.2 at 0.20 ppb for the 0.1 mbar step and -2.3 at 0.021 ppb for the 1 mbar step. This only corresponds to a $\sim 1\sigma$ detection of HCl, which at such a low significance level must be considered

dubious and is not robust. Furthermore, there are multiple unfitted features in the spectrum at a similar level, which do not correspond to any known spectral lines and are most likely due to noise. A more robust result is 3σ upper limits on HCl of 0.70 ppb for the 0.1 mbar step and 0.076 ppb for the 1 mbar step.

5. Discussion

Our HCl 3σ upper limits of 0.70 ppb (p<0.1 mbar) and 0.076 ppb (p<1 mbar) can be compared to other externally supplied stratospheric species to check the consistency of current theories on Neptune's external flux and chemistry. In particular we consider H_2O, CO, and CS, which are all believed to be externally sourced.

Stratospheric water is thought to mostly originate from the external flux of IDPs, so can be used to provide insight into expected external HCl, assuming both species are sourced from the same material. Feuchtgruber et al. (1997) measured a stratospheric H_2O volume mixing ratio of 1.5–3.5 ppb above an assumed condensation level at 0.55–0.7 mbar with Infrared Space Observatory (ISO) observations. More recent analysis of Herschel data by Lellouch et al. (2010) determined 0.85±0.20 ppb H_2O, assuming uniform mixing above a revised 1.2 mbar condensation level, which was based on an updated slightly warmer temperature profile than that used by Feuchtgruber et al. (1997). These measurements are consistent with estimates derived from IDP ablation modelling (Moses and Poppe, 2017), which have H_2O volume mixing ratio varying between ∼1 and 10 ppb in the 1 mbar–1 μbar range.

Therefore, an order of magnitude H_2O estimate suitable for our purposes

is uniformly mixed 1 ppb H_2O for pressures less than 1 mbar. Our HCl results can be compared to this by converting the 3σ HCl upper limit using the 1 mbar step profile into a 3σ upper limit on the Cl/O ratio of 0.076 ppb/1 ppb = 0.076, assuming all chlorine is in the form of HCl. This is equivalent to an upper limit of 230 times the solar Cl/O ratio of 3.3×10^{-4} from Lodders (2010). Measurements of IDP composition show chlorine is typically enriched by only 0.5–3 times the solar abundance (Arndt et al., 1996), so this upper limit is easily consistent with an IDP water source. The same calculation using our extremely speculative $\sim1\sigma$ detection of 0.021 ppb for the 1 mbar step profile would imply a Cl/O ratio of ∼64 times the solar Cl/O ratio. This is unreasonably high and if confirmed would require a significant additional chlorine source to that provided by IDPs.

Comet impacts provide an alternative and more sporadic source of external material into Neptune's stratosphere. Neptune's high stratospheric CO abundance of ∼1 ppm cannot be explained with the same steady state IDP flux that explains ∼1 ppb stratospheric water using any reasonable IDP composition (Moses and Poppe, 2017). A large comet impact is one solution to this discrepancy (Lellouch et al., 2005), as H_2O can be efficiently converted to CO by shock chemistry (Zahnle, 1996; Moses, 1996). Thus inputting large quantities of CO into Neptune's stratosphere without a correspondingly large amount of H_2O. A recent large impact is also consistent with observation of CS by Moreno et al. (2017) - a direct product of shock chemistry (Lellouch, 1996; Moses, 1996). Recent estimates place Neptune's stratospheric CO abundance at ∼1 ppm (Luszcz-Cook and de Pater, 2013; Teanby et al., 2019). If we ignore all HCl loss processes and assume HCl

is the dominant chlorine product from a comet impact then we can use our upper limits combined with the CO abundance to determine a Cl/O ratio upper limit of 0.076 ppb/1 ppm = 7.6×10^{-5}. Using the solar Cl/O ratio of 3.3×10^{-4} (Lodders, 2010) implies a stratospheric Cl/O ratio upper limit of 0.23 times solar. This sub-solar abundance is apparently inconsistent with an approximately solar composition comet. However, HCl is expected to have significant loss processes, resulting in a much lower overall atmospheric abundance, especially if the comet impact occurred a long time ago, so our upper limit is entirely consistent with an ancient comet impact. Furthermore, recent observations of comets (Bockelée-Morvan et al., 2014; Dhooghe et al., 2017) suggest HCl is depleted by a factor of ∼3–6 compared to solar composition, although chlorine could potentially be in other forms that convert to HCl in Neptune's atmosphere.

CS provides an example of a species that experiences significant stratospheric loss processes and provides an interesting comparison to HCl that can help explain the sub-solar Cl/O upper limit. The CS generated during the SL9 impact into Jupiter in 1994 (Lellouch, 1996; Moreno et al., 2003) still persists to this day, indicating it is moderately long-lived, but it has decayed by a factor of about ten in the 20+ years since the impact due to mixing and photochemical processes (Iino et al., 2016). On Neptune, Moreno et al. (2017) estimate a 4 km diameter comet impact occurring ∼1000 years ago is needed to explain Neptune's current CS abundance of ∼0.1 ppb above 0.1 mbar. Therefore, Neptune's current CS would be significantly depleted compared to its abundance just after the impact. The magnitude of this depletion can be estimated by assuming a solar composition comet with an S/O

ratio of ∼0.027 (Lodders, 2010), whereas the current stratospheric CS/CO ratio is around $\sim 10^{-4}$, implying an S/O ratio of $\sim 4 \times 10^{-3}$ times solar. In the unlikely event that HCl behaved exactly like CS, and combining the observed ∼0.1 ppb CS abundance with an assumed a solar Cl/S ratio of 0.0123 (Lodders, 2010), the HCl abundance would be approximately 1 ppt, much lower than our upper limit. This illustrates how HCl loss mechanisms have the potential to reduce abundances to undetectable levels, even if significant amounts are supplied sporadically by comets.

Further quantification of HCl loss processes is currently not possible as they are not included in photochemical models. Also many of the relevant reactions are not well understood. However, some qualitative discussion of potentially relevant processes is possible. A major loss mechanism for HCl is expected to be scavenging by aerosols (Showman, 2001; Teanby et al., 2014). While this mechanism is poorly constrained in giant planets, 1D diffusion modelling of Jupiter showed that scavenging can be an efficient loss process unless sticking coefficients between HCl and aerosol particles are unrealistically low (Teanby et al., 2014). On Neptune, aerosols are known to exist up to at least 1 mbar pressure levels (Irwin et al., 2011; Luszcz-Cook et al., 2016; Irwin et al., 2016; Moses et al., 1995), so could provide an efficient loss mechanism on Neptune too. Another potential reaction to remove HCl from Neptune's stratosphere is the so called "acetylene process" commonly used in industrial chemistry to combine C_2H_2 and HCl into chlorinated hydrocarbons such as polyvinyl chloride (PVC). Typically this reaction takes place at high temperature using metal catalyst substrates, but recent work shows that carbon-nitrogen compounds, such as those formed by photochemistry on

Neptune, could also provide viable catalysts (Xu and Luo, 2018). These reactions could be especially important within a high temperature impact plume. C_2H_2 and many other hydrocarbons have been observed in Neptune's atmosphere and provide the raw materials for such a process (Orton et al., 1987; Bezard et al., 1991; Fletcher et al., 2010; Greathouse et al., 2011).

Compared to other giant planets, our upper limit of 0.076 ppb (for p<1 mbar) is similar to the upper limit for Jupiter of 0.061 ppb, also derived from HIFI (Teanby et al., 2014). These results cannot unambiguously distinguish between potential HCl sources, but do suggest HCl abundances are extremely low in all giant planets as Jupiter and Neptune have the highest IDP fluxes (Moses and Poppe, 2017) and both have had fairly recent large comet impacts supplying additional material. Currently, photochemical models of Neptune (Moses et al., 2018; Dobrijevic et al., 2020) and Jupiter (Moses et al., 2005; Hue et al., 2018) do not include HCl or chlorine species. Inclusion of these species in more complex future models combined with remote or in-situ observations could allow further constraints on the external flux into these planets and possibly distinguish between external supply sources. However, a significant increase in sensitivity compared to the observations analysed here would be required.

6. Conclusion

Herschel HIFI observations of Neptune were used to determine upper limits on stratospheric HCl abundance. We found a 3σ upper limit of 0.076/0.70 ppb for a profile uniformly mixed at pressures less than 1/0.1 mbar respectively. The HCl upper limits provide useful constraints on Neptune's external flux

and are consistent with the modelled IDP flux and observations of other trace stratospheric species such as H_2O, CO, and CS. Our upper limit estimations are also consistent with a putative large comet impact in Neptune's recent past, provided that HCl loss mechanism are active in Neptune's stratosphere. Further constraints would require incorporation of chlorine species into photochemical models, although given the very low expected abundances, these constraints might be relatively modest.

7. Acknowledgements

NAT and PGJI are funded by the UK Science and Technology Facilities Council. HIFI has been designed and built by a consortium of institutes and university departments from across Europe, Canada and the United States under the leadership of SRON Netherlands Institute for Space Research, Groningen, The Netherlands and with major contributions from Germany, France and the US. Consortium members are: Canada: CSA, U.Waterloo; France: CESR, LAB, LERMA, IRAM; Germany: KOSMA, MPIfR, MPS; Ireland, NUI Maynooth; Italy: ASI, IFSI-INAF, Osservatorio Astrofisico di Arcetri-INAF; Netherlands: SRON, TUD; Poland: CAMK, CBK; Spain: Observatorio Astronómico Nacional (IGN), Centro de Astrobiología (CSIC-INTA). Sweden: Chalmers University of Technology - MC2, RSS & GARD; Onsala Space Observatory; Swedish National Space Board, Stockholm University - Stockholm Observatory; Switzerland: ETH Zurich, FHNW; USA: Caltech, JPL, NHSC.

References

Arndt, P., Bohsung, J., Maetz, M., Jessberger, E. K., 1996. The elemental abundances in interplanetary dust particles. Meteorit. Planet. Sci. 31 (6), 817–833.

Atreya, S. K., Hofstadter, M. H., In, J. H., Mousis, O., Reh, K., Wong, M. H., 2020. Deep atmosphere composition, structure, origin, and exploration, with particular focus on critical in situ science at the icy giants. Space Sci. Rev. 216 (1), 18.

Baines, K. H., Mickelson, M. E., Larson, L. E., Ferguson, D. W., 1995. The abundances of methane and ortho/para hydrogen on Uranus and Neptune: Implications of New Laboratory 4-0 H2 quadrupole line parameters. Icarus 114, 328–340.

Bezard, B., Romani, P. N., Conrath, B. J., Maguire, W. C., 1991. Hydrocarbons in Neptune's stratosphere from Voyager infrared observations. J. Geophys. Res. 96, 18961–18975.

Bockelée-Morvan, D., Biver, N., Crovisier, J., Lis, D. C., Hartogh, P., Moreno, R., de Val-Borro, M., Blake, G. A., Szutowicz, S., Boissier, J., Cernicharo, J., Charnley, S. B., Combi, M., Cordiner, M. A., de Graauw, T., Encrenaz, P., Jarchow, C., Kidger, M., Küppers, M., Milam, S. N., Müller, H. S. P., Phillips, T. G., Rengel, M., 2014. Searches for HCl and HF in comets 103P/Hartley 2 and C/2009 P1 (Garradd) with the Herschel Space Observatory. Astron. Astrophys. 562, A5.

Cavalié, T., Venot, O., Miguel, Y., Fletcher, L. N., Wurz, P., Mousis, O., Bounaceur, R., Hue, V., Leconte, J., Dobrijevic, M., 2020. The deep composition of Uranus and Neptune from in situ exploration and thermochemical modeling. Space Sci. Rev. 216 (4), 58.

Cavalié, T., Venot, O., Selsis, F., Hersant, F., Hartogh, P., Leconte, J., 2017. Thermochemistry and vertical mixing in the tropospheres of Uranus and Neptune: How convection inhibition can affect the derivation of deep oxygen abundances. Icarus 291, 1–16.

Conrath, B. J., Gautier, D., Owen, T. C., Samuelson, R. E., 1993. Constraints on N_2 in Neptune's atmosphere from Voyager measurements. Icarus 101, 168–171.

de Graauw, T., Helmich, F. P., Phillips, T. G., Stutzki, J., Caux, E., Whyborn, N. D., Dieleman, P., Roelfsema, P. R., Aarts, H., Assendorp, R., Bachiller, R., Baechtold, W., Barcia, A., Beintema, D. A., Belitsky, V., Benz, A. O., Bieber, R., Boogert, A., Borys, C., Bumble, B., Caïs, P., Caris, M., Cerulli-Irelli, P., Chattopadhyay, G., Cherednichenko, S., Ciechanowicz, M., Coeur-Joly, O., Comito, C., Cros, A., de Jonge, A., de Lange, G., Delforges, B., Delorme, Y., den Boggende, T., Desbat, J.-M., Diez-González, C., di Giorgio, A. M., Dubbeldam, L., Edwards, K., Eggens, M., Erickson, N., Evers, J., Fich, M., Finn, T., Franke, B., Gaier, T., Gal, C., Gao, J. R., Gallego, J.-D., Gauffre, S., Gill, J. J., Glenz, S., Golstein, H., Goulooze, H., Gunsing, T., Güsten, R., Hartogh, P., Hatch, W. A., Higgins, R., Honingh, E. C., Huisman, R., Jackson, B. D., Jacobs, H., Jacobs, K., Jarchow, C., Javadi, H., Jellema, W., Justen, M., Kar-

457 pov, A., Kasemann, C., Kawamura, J., Keizer, G., Kester, D., Klapwijk,
458 T. M., Klein, T., Kollberg, E., Kooi, J., Kooiman, P.-P., Kopf, B., Krause,
459 M., Krieg, J.-M., Kramer, C., Kruizenga, B., Kuhn, T., Laauwen, W.,
460 Lai, R., Larsson, B., Leduc, H. G., Leinz, C., Lin, R. H., Liseau, R., Liu,
461 G. S., Loose, A., López-Fernandez, I., Lord, S., Luinge, W., Marston, A.,
462 Martín-Pintado, J., Maestrini, A., Maiwald, F. W., McCoey, C., Mehdi,
463 I., Megej, A., Melchior, M., Meinsma, L., Merkel, H., Michalska, M., Mon-
464 stein, C., Moratschke, D., Morris, P., Muller, H., Murphy, J. A., Naber, A.,
465 Natale, E., Nowosielski, W., Nuzzolo, F., Olberg, M., Olbrich, M., Orfei,
466 R., Orleanski, P., Ossenkopf, V., Peacock, T., Pearson, J. C., Peron, I.,
467 Phillip-May, S., Piazzo, L., Planesas, P., Rataj, M., Ravera, L., Risacher,
468 C., Salez, M., Samoska, L. A., Saraceno, P., Schieder, R., Schlecht, E.,
469 Schlöder, F., Schmülling, F., Schultz, M., Schuster, K., Siebertz, O., Smit,
470 H., Szczerba, R., Shipman, R., Steinmetz, E., Stern, J. A., Stokroos, M.,
471 Teipen, R., Teyssier, D., Tils, T., Trappe, N., van Baaren, C., van Leeuwen,
472 B.-J., van de Stadt, H., Visser, H., Wildeman, K. J., Wafelbakker, C. K.,
473 Ward, J. S., Wesselius, P., Wild, W., Wulff, S., Wunsch, H.-J., Tielens,
474 X., Zaal, P., Zirath, H., Zmuidzinas, J., Zwart, F., 2010. The Herschel-
475 Heterodyne Instrument for the Far-Infrared (HIFI). Astron. Astrophys.
476 518, L6.

477 Dhooghe, F., De Keyser, J., Altwegg, K., Briois, C., Balsiger, H., Berthelier,
478 J.-J., Calmonte, U., Cessateur, G., Combi, M. R., Equeter, E., Fiethe,
479 B., Fray, N., Fuselier, S., Gasc, S., Gibbons, A., Gombosi, T., Gunell,
480 H., Hässig, M., Hilchenbach, M., Le Roy, L., Maggiolo, R., Mall, U.,
481 Marty, B., Neefs, E., Rème, H., Rubin, M., Sémon, T., Tzou, C.-Y.,

Wurz, P., 2017. Halogens as tracers of protosolar nebula material in comet 67P/Churyumov-Gerasimenko. Mon. Not. R. Astron. Soc. 472 (2), 1336–1345.

Dobrijevic, M., Loison, J. C., Hue, V., Cavalié, T., Hickson, K. M., 2020. 1D photochemical model of the ionosphere and the stratosphere of Neptune. Icarus 335, 1–14.

Fegley, B., Lodders, K., 1994. Chemical models of the deep atmospheres of Jupiter and Saturn. Icarus 110, 117–154.

Feuchtgruber, H., Lellouch, E., de Graauw, T., Bézard, B., Encrenaz, T., Griffin, M., 1997. External supply of oxygen to the atmospheres of the giant planets. Nature 389, 159–162.

Feuchtgruber, H., Lellouch, E., Orton, G., de Graauw, T., Vandenbussche, B., Swinyard, B., Moreno, R., Jarchow, C., Billebaud, F., Cavalié, T., Sidher, S., Hartogh, P., 2013. The D/H ratio in the atmospheres of Uranus and Neptune from Herschel-PACS observations. Astron. Astrophys. 551, 1–9.

Fletcher, L. N., Drossart, P., Burgdorf, M., Orton, G. S., Encrenaz, T., 2010. Neptune's atmospheric composition from AKARI infrared spectroscopy. Astron. Astrophys. 514, A17.

Fletcher, L. N., Swinyard, B., Salji, C., Polehampton, E., Fulton, T., Sidher, S., Lellouch, E., Moreno, R., Orton, G., Cavalié, T., Courtin, R., Rengel, M., Sagawa, H., Davis, G. R., Hartogh, P., Naylor, D., Walker, H.,

504 Lim, T., 2012. Sub-millimetre spectroscopy of Saturn's trace gases from
505 Herschel/SPIRE. Astron. Astrophys. 539, A44.

506 Fortney, J. J., Nettelmann, N., 2010. The interior structure, composition,
507 and evolution of giant planets. Space Sci. Rev. 152 (1-4), 423–447.

508 Fouchet, T., Orton, G., Irwin, P. G. J., Calcutt, S. B., Nixon, C. A., 2004.
509 Upper limits on hydrogen halides in Jupiter from Cassini/CIRS observa-
510 tions. Icarus 170, 237–241.

511 Goody, R. M., Yung, Y. L., 1989. Atmospheric Radiation: Theoretical Basis,
512 2nd Edition. Oxford University Press, Oxford.

513 Greathouse, T. K., Richter, M., Lacy, J., Moses, J., Orton, G., Encrenaz,
514 T., Hammel, H. B., Jaffe, D., 2011. A spatially resolved high spectral
515 resolution study of Neptune's stratosphere. Icarus 214 (2), 606–621.

516 Helled, R., Anderson, J. D., Podolak, M., Schubert, G., 2011. Interior Models
517 of Uranus and Neptune. Astrophys. J. 726, 1–7.

518 Helled, R., Nettelmann, N., Guillot, T., 2020. Uranus and Neptune: origin,
519 evolution and internal structure. Space Sci. Rev. 216 (3), 38.

520 Helled, R., Stevenson, D., 2017. The fuzziness of giant planets' cores. Astro-
521 phys. J. Lett. 840 (1), L4.

522 Hesman, B. E., Davis, G. R., Matthews, H. E., Orton, G. S., 2007. The
523 abundance profile of CO in Neptune's atmosphere. Icarus 186, 342–353.

524 HIFI Observers' Manual, June 2011. HERSCHEL-HSC-DOC-0784. Version
525 2.4, http://herschel.esac.esa.int/Docs/HIFI/pdf/hifi_om.pdf.

Hue, V., Hersant, F., Cavalié, T., Dobrijevic, M., Sinclair, J. A., 2018. Photochemistry, mixing and transport in Jupiter's stratosphere constrained by Cassini. Icarus 307, 106–123.

Iino, T., Ohyama, H., Hirahara, Y., Takahashi, T., Tsukagoshi, T., 2016. Submillimeter observation of Jupiter's stratospheric composition: Detection of carbon monosulfide (J=7-6) 19 years after the cometary impact. Astron. J. 152 (6), 1–5.

Irwin, P., Teanby, N., de Kok, R., Fletcher, L., Howett, C., Tsang, C., Wilson, C., Calcutt, S., Nixon, C., Parrish, P., 2008. The NEMESIS planetary atmosphere radiative transfer and retrieval tool. J. Quant. Spectro. Rad. Trans. 109, 1136–1150.

Irwin, P. G. J., 2009. Giant planets of our solar system: atmospheres, composition, and structure, 2nd Edition. Springer-Praxis, Chichester UK.

Irwin, P. G. J., Fletcher, L. N., Tice, D., Owen, S. J., Orton, G. S., Teanby, N. A., Davis, G. R., 2016. Time variability of Neptune's horizontal and vertical cloud structure revealed by VLT/SINFONI and Gemini/NIFS from 2009 to 2013. Icarus 271, 418–437.

Irwin, P. G. J., Teanby, N. A., Davis, G. R., Fletcher, L. N., Orton, G. S., Tice, D., Hurley, J., Calcutt, S. B., 2011. Multispectral imaging observations of Neptune's cloud structure with Gemini-North. Icarus 216, 141–158.

Irwin, P. G. J., Toledo, D., Braude, A. S., Bacon, R., Weilbacher, P. M., Teanby, N. A., Fletcher, L. N., Orton, G. S., 2019a. Latitudinal variation

in the abundance of methane (CH_4) above the clouds in Neptune's atmosphere from VLT/MUSE Narrow Field Mode Observations. Icarus 331, 69–82.

Irwin, P. G. J., Toledo, D., Garland, R., Teanby, N. A., Fletcher, L. N., Orton, G. S., Bézard, B., 2019b. Probable detection of hydrogen sulphide (H_2S) in Neptune's atmosphere. Icarus 321, 550–563.

Karkoschka, E., Tomasko, M. G., 2011. The haze and methane distributions on Neptune from HST-STIS spectroscopy. Icarus 211 (1), 780–797.

Kaye, J. A., Strobel, D. F., 1983. HCN formation on Jupiter - The coupled photochemistry of ammonia and Acetylene. Icarus 54, 417–433.

Kester, D., Avruch, I., Teyssier, D., 2014. Correction of electric standing waves. In: Bayesian Inference and Maximum Entropy Methods in Science and Engineering. Vol. 1636 of Amer. Inst. Phys. Conf. Series. pp. 62–67.

Lacis, A. A., Oinas, V., 1991. A description of the correlated k distribution method for modeling nongray gaseous absorption, thermal emission, and multiple-scattering in vertically inhomogeneous atmospheres. J. Geophys. Res. 96 (D5), 9027–9063.

Lellouch, E., 1996. Chemistry induced by the impacts: Observations. In: Noll, K. S., Weaver, H. A., Feldman, P. D. (Eds.), IAU Colloq. 156: The Collision of Comet Shoemaker-Levy 9 and Jupiter. pp. 213–241.

Lellouch, E., Hartogh, P., Feuchtgruber, H., Vandenbussche, B., de Graauw, T., Moreno, R., Jarchow, C., Cavalié, T., Orton, G., Banaszkiewicz, M.,

570 Blecka, M. I., Bockelée-Morvan, D., Crovisier, J., Encrenaz, T., Fulton, T.,
571 Küppers, M., Lara, L. M., Lis, D. C., Medvedev, A. S., Rengel, M., Sagawa,
572 H., Swinyard, B., Szutowicz, S., Bensch, F., Bergin, E., Billebaud, F.,
573 Biver, N., Blake, G. A., Blommaert, J. A. D. L., Cernicharo, J., Courtin,
574 R., Davis, G. R., Decin, L., Encrenaz, P., Gonzalez, A., Jehin, E., Kidger,
575 M., Naylor, D., Portyankina, G., Schieder, R., Sidher, S., Thomas, N., de
576 Val-Borro, M., Verdugo, E., Waelkens, C., Walker, H., Aarts, H., Comito,
577 C., Kawamura, J. H., Maestrini, A., Peacocke, T., Teipen, R., Tils, T.,
578 Wildeman, K., Jul. 2010. First results of Herschel-PACS observations of
579 Neptune. Astron. Astrophys. 518, L152.

580 Lellouch, E., Moreno, R., Orton, G. S., Feuchtgruber, H., Cavalié, T., Moses,
581 J. I., Hartogh, P., Jarchow, C., Sagawa, H., Jul. 2015. New constraints on
582 the CH_4 vertical profile in Uranus and Neptune from Herschel observations.
583 Astron. Astrophys., A121.

584 Lellouch, E., Moreno, R., Paubert, G., 2005. A dual origin for Neptune's
585 carbon monoxide? Astron. Astrophys. 430, L37–L40.

586 Lindal, G. F., 1992. The atmosphere of Neptune - an analysis of radio occul-
587 tation data acquired with Voyager 2. Astron. J. 103, 967–982.

588 Lodders, K., 2010. Solar system abundances of the elements. In: Goswami,
589 A., Reddy, B. E. (Eds.), Principles and Perspectives in Cosmochemistry.
590 Springer Berlin Heidelberg, Berlin, Heidelberg, pp. 379–417.

591 Lodders, K., Fegley, Jr., B., 1994. The origin of carbon monoxide in Nep-
592 tunes's atmosphere. Icarus 112, 368–375.

593 Luszcz-Cook, S. H., de Kleer, K., de Pater, I., Adamkovics, M., Hammel,
594 H. B., 2016. Retrieving Neptune's aerosol properties from Keck OSIRIS
595 observations. I. Dark regions. ic 276, 52–87.

596 Luszcz-Cook, S. H., de Pater, I., 2013. Constraining the origins of Neptune's
597 carbon monoxide abundance with CARMA millimeter-wave observations.
598 Icarus 222, 379–400.

599 Marten, A., Matthews, H. E., Owen, T., Moreno, R., Hidayat, T., Biraud, Y.,
600 2005. Improved constraints on Neptune's atmosphere from submillimetre-
601 wavelength observations. Astron. Astrophys. 429, 1097–1105.

602 Moreno, R., 2010. OT1_rmoreno_2: Probing the atmospheres of Uranus, Nep-
603 tune and Titan with CH4 lines. Herschel Space Observatory Proposal.

604 Moreno, R., Lellouch, E., Cavalié, T., Moullet, A., 2017. Detection of CS in
605 Neptune's atmosphere from ALMA observations. Astron. Astrophys. 608,
606 L5.

607 Moreno, R., Lellouch, E., Lara, L. M., Courtin, R., Bockelée-Morvan, D.,
608 Hartogh, P., Rengel, M., Biver, N., Banaszkiewicz, M., González, A., 2011.
609 First detection of hydrogen isocyanide (HNC) in Titan's atmosphere. As-
610 tron. Astrophys. 536, L12.

611 Moreno, R., Marten, A., Matthews, H. E., Biraud, Y., 2003. Long-term evolu-
612 tion of CO, CS and HCN in Jupiter after the impacts of comet Shoemaker-
613 Levy 9. Plan. & Space Sci. 51, 591–611.

614 Moses, J., 2000. Photochemistry in Giant-Planet Atmospheres. In: Griffith,

615 C. A., Marley, M. S. (Eds.), From Giant Planets to Cool Stars. Vol. 212
616 of Astronomical Society of the Pacific Conference Series. pp. 196–206.

617 Moses, J. I., 1992. Meteoroid ablation in Neptune's atmosphere. Icarus 99,
618 368–383.

619 Moses, J. I., 1996. SL9 impact chemistry: Long-term photochemical evolu-
620 tion. In: Noll, K. S., Weaver, H. A., Feldman, P. D. (Eds.), IAU Colloq.
621 156: The Collision of Comet Shoemaker-Levy 9 and Jupiter. pp. 243–268.

622 Moses, J. I., Allen, M., Gladstone, G. R., 1995. Nitrogen and oxygen photo-
623 chemistry following SL9. Geophys. Res. Lett. 22, 1601–1604.

624 Moses, J. I., Fletcher, L. N., Greathouse, T. K., Orton, G. S., Hue, V., 2018.
625 Seasonal stratospheric photochemistry on Uranus and Neptune. Icarus 307,
626 124–145.

627 Moses, J. I., Fouchet, T., Bézard, B., Gladstone, G. R., Lellouch, E., Feucht-
628 gruber, H., Aug. 2005. Photochemistry and diffusion in Jupiter's strato-
629 sphere: Constraints from ISO observations and comparisons with other
630 giant planets. J. Geophys. Res. 110, 8001.

631 Moses, J. I., Poppe, A. R., 2017. Dust ablation on the giant planets: Conse-
632 quences for stratospheric photochemistry. Icarus 297, 33–58.

633 Mousis, O., Aguichine, A., Atkinson, D. H., Atreya, S. K., Cavalié, T., Lu-
634 nine, J. I., Mand t, K. E., Ronnet, T., 2020. Key atmospheric signatures
635 for identifying the source reservoirs of volatiles in Uranus and Neptune.
636 Space Sci. Rev. 216 (5), 77.

637 Nettelmann, N., Helled, R., Fortney, J. J., Redmer, R., 2013. New indication
638 for a dichotomy in the interior structure of Uranus and Neptune from the
639 application of modified shape and rotation data. Plan. & Space Sci. 77,
640 143–151.

641 Orton, G. S., Aitken, D. K., Smith, C., Roche, P. F., Caldwell, J., Snyder,
642 R., 1987. The spectra of Uranus and Neptune at 8-14 and 17-23 μm. Icarus
643 70 (1), 1–12.

644 Owen, T., Encrenaz, T., 2006. Compositional constraints on giant planet
645 formation. Plan. & Space Sci. 54, 1188–1196.

646 Pilbratt, G. L., Riedinger, J. R., Passvogel, T., Crone, G., Doyle, D., Gageur,
647 U., Heras, A. M., Jewell, C., Metcalfe, L., Ott, S., Schmidt, M., 2010. Her-
648 schel Space Observatory. An ESA facility for far-infrared and submillimetre
649 astronomy. Astron. Astrophys. 518, L1.

650 Press, W. H., Flannery, B. P., Teukolsky, S. A., Vetterling, W. T., 1992.
651 Numerical Recipes, 2nd Edition. Cambridge Univ. Press, Cambridge UK.

652 Roelfsema, P. R., Helmich, F. P., Teyssier, D., Ossenkopf, V., Morris, P.,
653 Olberg, M., Shipman, R., Risacher, C., Akyilmaz, M., Assendorp, R.,
654 Avruch, I. M., Beintema, D., Biver, N., Boogert, A., Borys, C., Braine,
655 J., Caris, M., Caux, E., Cernicharo, J., Coeur-Joly, O., Comito, C., de
656 Lange, G., Delforge, B., Dieleman, P., Dubbeldam, L., de Graauw, T.,
657 Edwards, K., Fich, M., Flederus, F., Gal, C., di Giorgio, A., Herpin, F.,
658 Higgins, D. R., Hoac, A., Huisman, R., Jarchow, C., Jellema, W., de Jonge,
659 A., Kester, D., Klein, T., Kooi, J., Kramer, C., Laauwen, W., Larsson,

660 B., Leinz, C., Lord, S., Lorenzani, A., Luinge, W., Marston, A., Martín-
661 Pintado, J., McCoey, C., Melchior, M., Michalska, M., Moreno, R., Müller,
662 H., Nowosielski, W., Okada, Y., Orleański, P., Phillips, T. G., Pearson, J.,
663 Rabois, D., Ravera, L., Rector, J., Rengel, M., Sagawa, H., Salomons, W.,
664 Sánchez-Suárez, E., Schieder, R., Schlöder, F., Schmülling, F., Soldati,
665 M., Stutzki, J., Thomas, B., Tielens, A. G. G. M., Vastel, C., Wildeman,
666 K., Xie, Q., Xilouris, M., Wafelbakker, C., Whyborn, N., Zaal, P., Bell,
667 T., Bjerkeli, P., De Beck, E., Cavalié, T., Crockett, N. R., Hily-Blant, P.,
668 Kama, M., Kaminski, T., Leflóch, B., Lombaert, R., de Luca, M., Makai,
669 Z., Marseille, M., Nagy, Z., Pacheco, S., van der Wiel, M. H. D., Wang,
670 S., Yıldız, U., Jan. 2012. In-orbit performance of Herschel-HIFI. Astron.
671 Astrophys. 537, A17.

672 Shipman, R. F., Beaulieu, S. F., Teyssier, D., Morris, P., Rengel, M., Mc-
673 Coey, C., Edwards, K., Kester, D., Lorenzani, A., Coeur-Joly, O., Mel-
674 chior, M., Xie, J., Sanchez, E., Zaal, P., Avruch, I., Borys, C., Braine, J.,
675 Comito, C., Delforge, B., Herpin, F., Hoac, A., Kwon, W., Lord, S. D.,
676 Marston, A., Mueller, M., Olberg, M., Ossenkopf, V., Puga, E., Akyilmaz-
677 Yabaci, M., Dec. 2017. Data processing pipeline for Herschel HIFI. Astron.
678 Astrophys. 608, A49.

679 Showman, A. P., 2001. Hydrogen halides on Jupiter and Saturn. Icarus 152,
680 140–150.

681 Teanby, N., Irwin, P., Moses, J., Helled, R., 2020. Neptune and Uranus: ice
682 or rock giants? Phil. Trans. R. Soc. Lond. A under review.

683 Teanby, N. A., Fletcher, L. N., Irwin, P. G. J., Fouchet, T., Orton, G. S.,

2006. New upper limits for hydrogen halides on Saturn derived from Cassini-CIRS data. Icarus 185, 466–475.

Teanby, N. A., Irwin, P. G. J., Moses, J. I., 2019. Neptune's carbon monoxide profile and phosphine upper limits from Herschel/SPIRE: Implications for interior structure and formation. Icarus 319, 86–98.

Teanby, N. A., Irwin, P. G. J., Nixon, C. A., Courtin, R., Swinyard, B. M., Moreno, R., Lellouch, E., Rengel, M., Hartogh, P., 2013. Constraints on Titan's middle atmosphere ammonia abundance from Herschel/SPIRE submillimetre spectra. Plan. & Space Sci. 75, 136–147.

Teanby, N. A., Showman, A. P., Fletcher, L. N., Irwin, P. G. J., 2014. Constraints on Jupiter's stratospheric HCl abundance and chlorine cycle from Herschel/HIFI. Plan. & Space Sci. 103, 250–261.

Tollefson, J., de Pater, I., Luszcz-Cook, S., DeBoer, D., 2019. Neptune's latitudinal variations as viewed with ALMA. Astron. J. 157 (6), 251.

Venot, O., Cavalié, T., Bounaceur, R., Tremblin, P., Brouillard, L., Lhoussaine Ben Brahim, R., 2020. New chemical scheme for giant planet thermochemistry. Update of the methanol chemistry and new reduced chemical scheme. Astron. Astrophys. 634, A78.

Xu, H., Luo, G., 2018. Green production of pvc from laboratory to industrialization: State-of-the-art review of heterogeneous non-mercury catalysts for acetylene hydrochlorination. Journal of Industrial and Engineering Chemistry 65, 13–25.

706 Zahnle, K., 1996. Dynamics and chemistry of SL9 plumes. In: Noll, K. S.,
707 Weaver, H. A., Feldman, P. D. (Eds.), IAU Colloq. 156: The Collision of
708 Comet Shoemaker-Levy 9 and Jupiter. pp. 183–212.

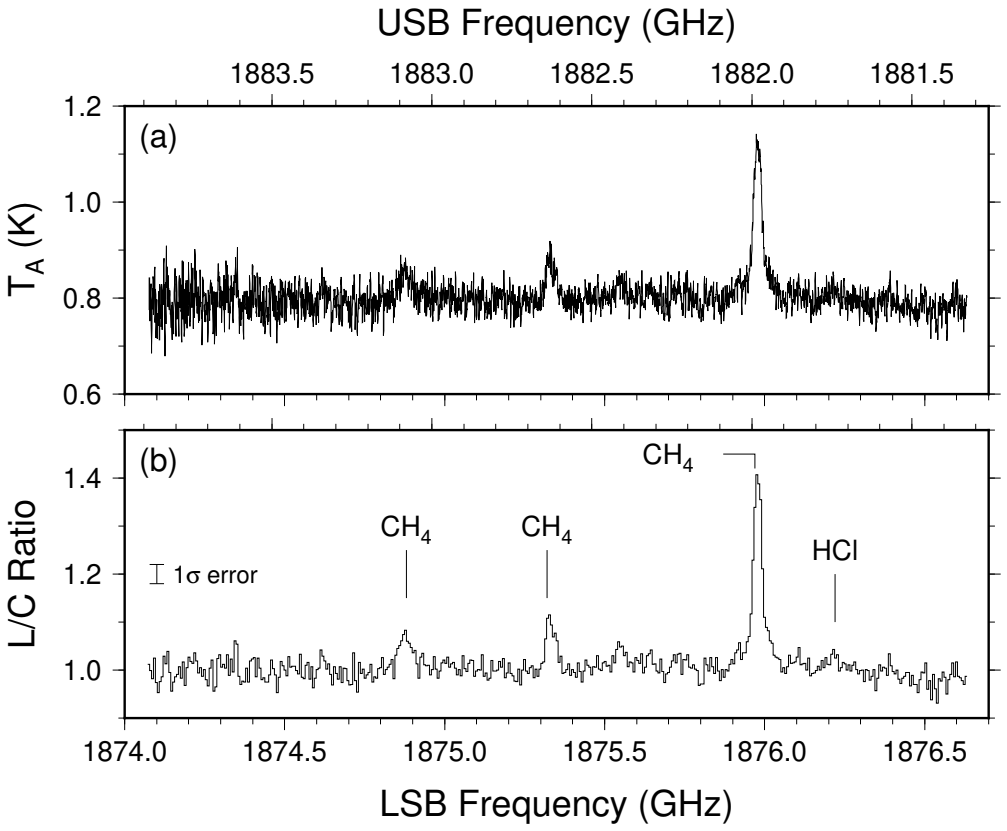

Figure 1: HIFI band 7 disc-averaged observations of Neptune. (a) Level 2.5 double side band (DSB) spectrum from the Herschel Science Archive at 1.1 MHz spectral resolution. Spectrum is the average of horizontal and vertical polarisations. (b) DSB spectrum convolved with a 6 MHz width bin to improve signal-to-noise and converted to a line-to-continuum ratio to simplify analysis. 1σ standard error shown. CH_4 emission features are in the upper side band (USB) and were the original target of the observation (Lellouch et al., 2015), HCl line position is in the lower side band (LSB).

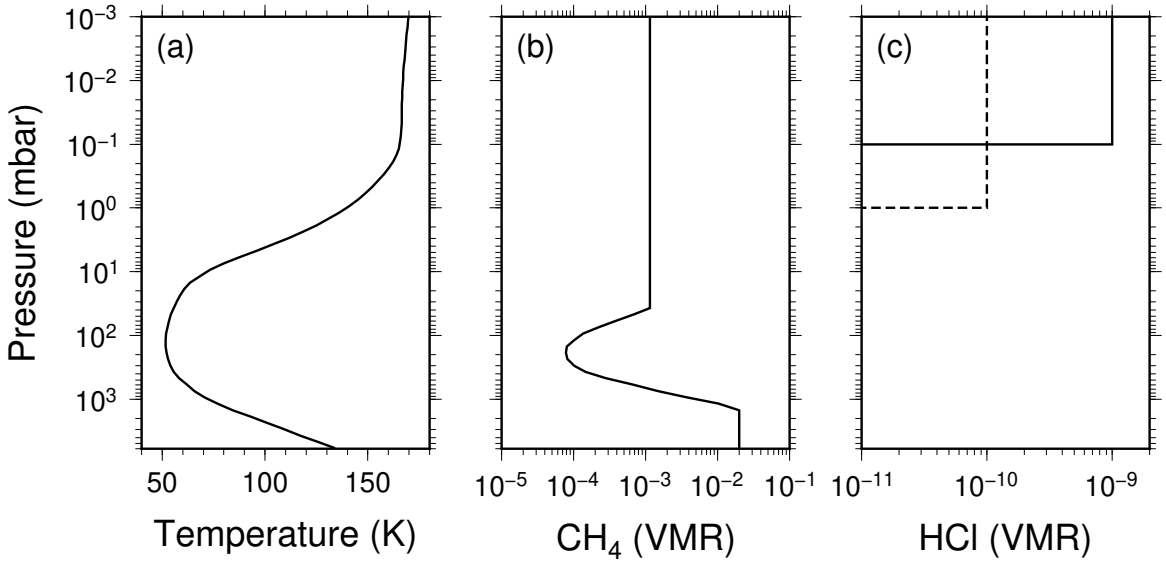

Figure 2: Atmospheric profiles used to model the HIFI Neptune spectrum. (a) Temperature profile based on Lindal (1992) and Fletcher et al. (2010). (b) Methane profile from Lellouch et al. (2015). (c) Nominal initial step profiles used to model HCl emission.

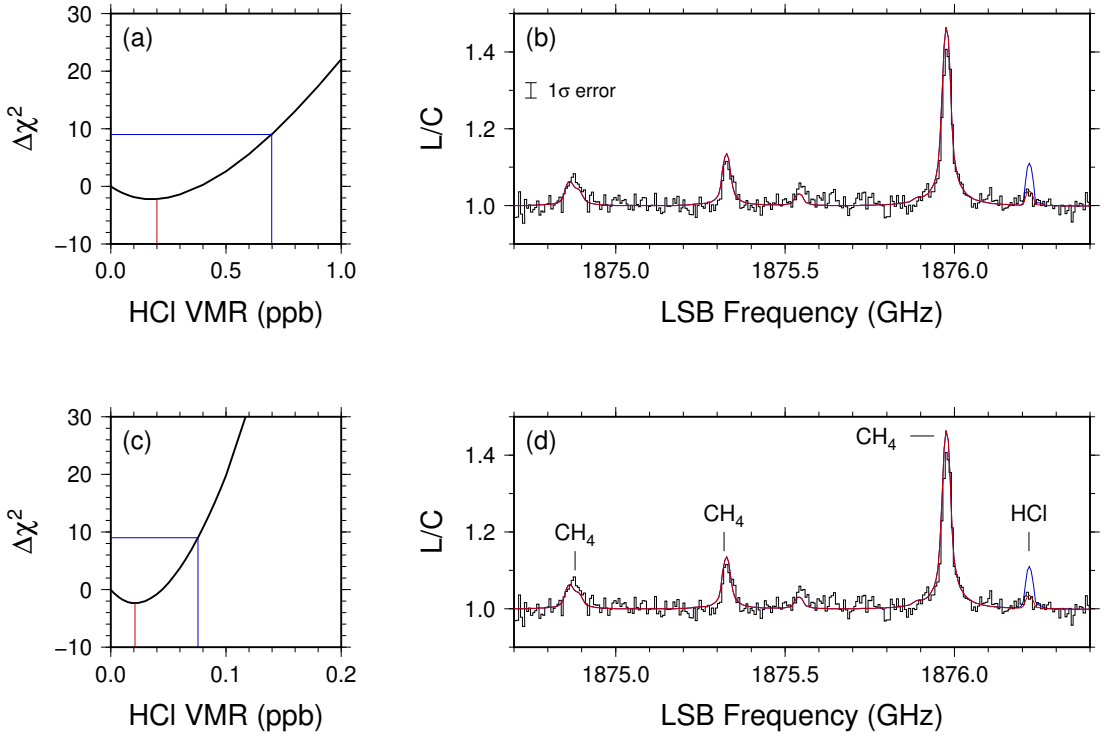

Figure 3: Fits to the HIFI spectrum. (a) $\Delta\chi^2$ as a function of HCl volume mixing ratio (VMR) for a uniform profile at pressures less than 0.1 mbar. Red line indicates minimum and best fitting abundance, whereas blue line indicates 3σ upper limit. (b) Fits to the data using the best fitting HCl profile (red) and 3σ upper limit (blue). (c,d) Show the same analysis for a 1 mbar pressure cut off. The $\Delta\chi^2$ minima are not deep enough to be considered significant, making these 3σ upper limits of 0.70 ppb for the 0.1 mbar profile and 0.076 ppb for the 1 mbar profile. CH_4 emission features (folded in from the upper side band) are well fitted using the reference profile from Lellouch et al. (2015).